Hidden variable in the electrocaloric effect of ferroics

Ravi Kashikar,[1,*,†] Subhashree Chatterjee,[2,†] Folarin Shola Taofeek,[1] Abhisikta Barman,[2] Shubhankar Barman,[3] Sohini Kar-Narayan,[4] Anuja Datta,[3,4] Sergey Lisenkov,[1] Devajyoti Mukherjee,[2,‡] and I. Ponomareva[1,§]

[1]*Department of Physics, University of South Florida, Tampa, Florida 33620, USA*

[2]*School of Physical Sciences, Indian Association for the Cultivation of Science, 2A & 2B Raja S. C. Mullick Road, Kolkata 700032, India*

[3]*School of Applied and Interdisciplinary Sciences, Indian Association for the Cultivation of Science, 2A & 2B Raja S. C. Mullick Road, Kolkata 700032, India*

[4]*Department of Materials Science & Metallurgy, University of Cambridge, 27 Charles Babbage Road, Cambridge CB3 0FS, United Kingdom*

(Received 4 March 2022; revised 7 September 2022; accepted 8 November 2022; published 5 December 2022)

Caloric effects allow for temperature control through adiabatic application of external fields and are actively explored for solid-state refrigeration. The common wisdom is that the application of ultrahigh fields enhances the effects, thus providing a route to their practical applications. Using the ferroelectric relaxor (Ba, Ca)(Ti, Zr)O_3, we demonstrate that in ferroics, which are the prime candidates for such application, this is not true in general and that caloric effects can be enhanced through the reduction of the applied field. The explanation of such a counterintuitive response is in the dependence of the electrocaloric effect on the effective poling field that can be regarded as a "hidden" variable of the caloric effects.

DOI: 10.1103/PhysRevMaterials.6.124403

I. INTRODUCTION

Caloric effects are under active investigation owing to the groundbreaking findings of giant caloric effects in ferroics [1–12] and their promise for solid-state coolers that are energetically efficient and environmentally friendly alternatives to conventional refrigeration [13,14]. The effect is defined as the reversible change in temperature under adiabatic application of electric, magnetic, or stress fields. For example, the electrocaloric effect is associated with a reversible change in temperature under adiabatic application of electric field and can be quantified with the help of thermodynamics, in particular, Maxwell's equation:

$$\Delta T \approx -\frac{T}{\rho C_E}\int_{E_1}^{E_2}\left(\frac{\partial P}{\partial T}\right)_E dE, \tag{1}$$

where P, T, and C_E are polarization, temperature, and specific heat at constant electric field, respectively, while E and ρ are the electric field and materials density, and E_1 and E_2 are the initial and final values of the applied electric field. Typically, electrocaloric effects are rather small (on the order of a Kelvin under applied fields of 10–40 kV/cm) for practical applications. However, Eq. (1) suggests that electrocaloric ΔT can be increased by the application of large electric fields E_2, which is only possible in high-quality samples. Indeed, the groundbreaking approach of using high-quality thin films to achieve a giant electrocaloric effect through application of high electric fields [1] has promoted an unprecedented research interest in electrocaloric effects with the number of publications increasing exponentially in the last decade [7]. More precisely, in Ref. [1] application of an electric field of up to 776 kV/cm to poled antiferroelectric Pb(Ti, Zr)O_3 films was predicted to yield a 12 K change in temperature [1]. The followup studies reported that in a multilayer-thick film of ferroelectric $BaTiO_3$, application of 800 kV/cm resulted in a 7.1 K change in temperature [15]. $Ba_{0.8}Sr_{0.2}TiO_3$ films exhibited an electrocaloric value of ΔT of 9.1 K under the field of 1000 kV/cm [16], while $BaZr_{0.2}Ti_{0.8}O_3$ [17] thin films were reported to produce a 43.6 K temperature change under an electric field of 1011 kV/cm. Furthermore, in polymer/$Ba_{0.67}Sr_{0.33}TiO_3$ nanocomposites the field of 1500 kV/cm yielded a 32 K change in temperature [18]. Although the field of electrocaloric measurements is often faulted by the reproducibility issues, still an inspection of over 36 studies compiled in Ref. [7] suggests that the general trend is in agreement with expectation from Eq. (1), that is, larger fields lead to larger electrocaloric ΔT. This can be further illustrated in the case of ferroelectric polymers where a nearly linear increase in ΔT with electric field was reported [18].

Here we grew a high-quality epitaxial thin film of ferroelectric $(Ba_{0.85}Ca_{0.15})(Ti_{0.9}Zr_{0.1})O_3$ (BCZT) which allowed for the application of ultrahigh electric fields up to 1000 kV/cm. Surprisingly, we found that (i) such films remain in the ferroelectric phase up to 140 K above the Curie point ($T_C = 360$ K) of their bulk counterpart, and (ii) the application of ultrahigh electric fields suppresses the electrocaloric effect. With the help of first-principles-based simulations, we reveal that there exists a "hidden" variable in the caloric effects of ferroics that is responsible for the aforementioned findings and which can be manipulated to tune an electrocaloric effect in a very counterintuitive way. For example, we demonstrate that in a given temperature range the largest electrocaloric

*ravik@usf.edu
†These authors contributed equally to this work.
‡sspdm@iacs.res.in
§iponomar@usf.edu

change in temperatures is enhanced by a factor of seven through a two times *decrease* of the electric field.

II. METHODS

A dense ceramic target of $(Ba_{0.85}Ca_{0.15})(Ti_{0.9}Zr_{0.1})O_3$ (BCZT) was prepared by a conventional solid-state reaction starting from high-purity (99.99%) powders. The details of the bulk BCZT ceramic preparation is provided in the Supplemental Material [19]. The as-prepared BCZT bulk ceramic was characterized for phase purity, structural refinement, and chemical composition using x-ray diffraction (XRD), energy-dispersive spectroscopy (EDS), x-ray photoelectron spectroscopy (XPS), and Raman spectroscopy (see Fig. S1 in the Supplemental Material [19] and also Refs. [20,21]). Temperature-dependent dielectric and ferroelectric measurements of the bulk pellet were conducted with a planar capacitor structure using sputtered Au top and bottom electrodes (see Fig. S2 in the Supplemental Material [19]).

An epitaxial BCZT thin-film heterostructure using $La_{0.7}Sr_{0.3}MnO_3$ (LSMO) top and bottom electrodes was fabricated on a single-crystal $SrTiO_3$ (STO) (100) substrate using a commercial pulsed laser deposition (PLD) system. The details of the thin-film fabrication and characterization are provided in the Supplemental Material [19]. The crystallinity, strain, composition, surface morphology, and interfacial microstructures of the BCZT/LSMO heterostructure were investigated using symmetric/asymmetric XRD, EDS, XPS, atomic force microscopy (AFM), and high-resolution transmission electron microscopy (HRTEM) (see Figs. S3 and S4 in the Supplemental Material [19]). Temperature-dependent dielectric measurements of the LSMO/BCZT/LSMO thin-film capacitor were conducted in the frequency range of 1 kHz to 1 MHz by using a precision digital LCR meter (see Fig. S5 in the Supplemental Material [19]). Temperature-dependent ferroelectric hysteresis loops for the BCZT thin film were measured using a commercial ferroelectric test system (Radiant Technologies Inc.) equipped with a microprobe station at a frequency of 1 kHz in different ranges of electric fields from [–400:400] kV/cm to [–1000:1000] kV/cm.

Computationally, we model bulk $Ba(Ti_{1-x}, Zr_x)O_3$ using a first-principles-based effective Hamiltonian of Ref. [22]. We chose $Ba(Ti_{0.9}, Zr_{0.1})O_3$ as the closest material to (Ba, Ca)(Ti, Zr)O_3 for which a reliable computational approach is available. The degrees of freedom for the Hamiltonian include local soft modes which are proportional to the local dipole moments and local strain variables that describe deformation of the unit cells. The Hamiltonian includes the interactions that are responsible for the ferroelectricity in $Ba(Ti_{1-x}, Zr_x)O_3$: local mode self-energy up to fourth order, harmonic short- and long-range interactions between the local modes, elastic deformations, and interactions responsible for the electrostriction, and the term that describes interaction of local modes with the electric field. The Hamiltonian reproduces correctly the complex phase diagram of temperature vs Zr concentration in $BaTiO_3$ [22]. Note that $Ba(Ti_{1-x}, Zr_x)O_3$ bulk is simulated by applying periodic boundary conditions along all three Cartesian directions. To model hysteresis loops, the effective Hamiltonian is used within the framework of classical molecular dynamics (MD) with an Evans-Hoover thermostat [23] to simulate the NPT ensemble. The integration step is 1 fs. The ac electric field is simulated with amplitudes of 50, 500, and 5000 kV/cm and frequency 0.01 THz. Technically, three periods of the field are simulated and the data are then averaged. The simulation supercell size is $30 \times 30 \times 30$ unit cells of perovskite. The hysteresis loops are simulated for the temperature interval from 300 to 510 K in steps of 10 K.

To compute electrocaloric change in temperature, we integrate Eq. (1) numerically; for that, hysteresis loops $P(E)$ in the first quadrant are used to compute $P(T, E)$ dependencies. Technically, for a given E we first fit $P(T)$ dependencies and then compute the analytical derivative $(\frac{\partial P}{\partial T})_E$, which is then used to integrate Eq. (1) numerically using Simpson's method as implemented in the SciPy module [24]. We found that fitting of $(\frac{\partial P}{\partial T})_E$ has a crucial role and can introduce spurious peaks and lead to incorrect predictions for ΔT. One way to avoid the artifacts is to compare the predictions from the fitted data with those of unfitted data, that is, when the aforementioned derivative is computed numerically. We empirically found that sometimes fitting with the nth-order polynomial works well, while sometimes we have to use spline fitting [24]. In all cases the reported data have been properly validated by comparison with the numerical derivative approach. We have used the experimental value for heat capacity $C = 540$ J/kg K [25].

To simulate the electrocaloric effect directly we used both adiabatic and isothermal simulations. The adiabatic simulations were carried out using our original semiclassical approach, that is, the isentropic Monte Carlo that incorporates the quantum-mechanical effect into the heat capacity [26]. The simulation supercell cell was $16 \times 16 \times 16$. We first simulate hysteresis loops using Metropolis Monte Carlo and then use zero-field structures to initialize direct adiabatic simulations. In the latter simulations the electric field was slowly increased from 0 to E_0 kV/cm and then decreased back to zero at a rate of E_0/N_{MC} kV/cm per one Monte Carlo sweep. Here $N_{MC} = 100\,000$ is the number of Monte Carlo (MC) sweeps used for the field application. This cycle of field application has been repeated twice so that the electrocaloric change in temperature can be investigated in the second cycle, after the simulated sample already experienced the field E_0. For the isothermal simulations we used MD with the supercell of $30 \times 30 \times 30$ following the computational approach of Ref. [27]. Note that the difference between the supercell size between the two simulations is due to the difference in the computational efficiency of MD and Monte Carlo simulations (with the former one being much faster). In this simulation we simulate the ac electric field with amplitudes in the range 50–10 000 kV/cm and frequency of 0.5 GHz. The computations allow one to harvest isothermal heat which can then be converted into adiabatic temperature change $\Delta T = Q/C$. We focus only on the reversible parts of the simulations.

III. RESULTS AND DISCUSSION

We begin with the electrocaloric effect in the bulk BCZT ceramic. Figure 1(a) shows the ferroelectric hysteresis loops

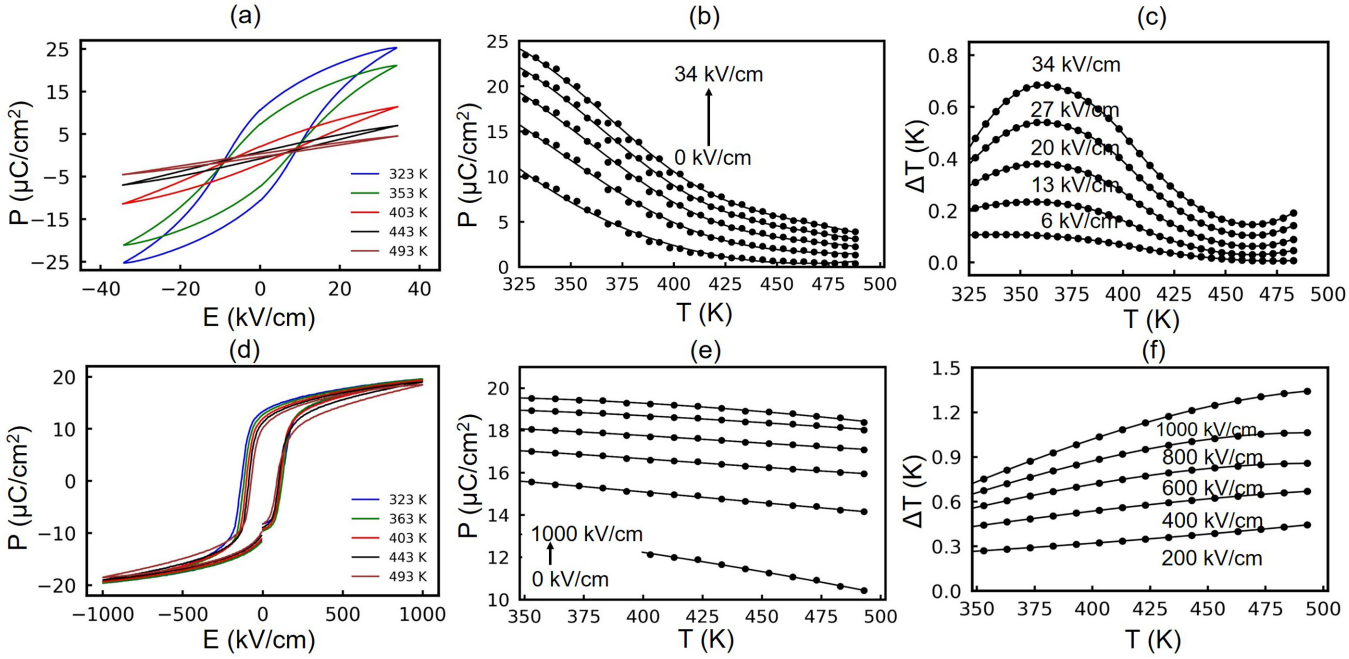

FIG. 1. Polarization as a function of applied electric field (a), temperature (b), and electrocaloric change in temperature as a function of temperature in bulk BCZT (c). Panels (d)–(f) present the same dependencies but for 100-nm-thick BCZT film.

obtained at different temperatures. The largest field that we were able to apply to the sample was 34 kV/cm. The hysteresis loops data were used to get the dependencies of the electric polarization on temperature for different electric fields [see Fig. 1(b)], which are then employed in the framework of the indirect approach of Eq. (1) to estimate the electrocaloric change in temperature as detailed in Sec. II. For this study we use $E_1 = 0$ kV/cm and $E_2 = \Delta E$. The electrocaloric change in temperature is given in Fig. 1(c). The peak in ΔT occurs at 363 K, which is near the location of maximum in the temperature dependence of the dielectric constant (see Fig. S2 in the Supplemental Material [19]). The latter maximum is at 360 K and typically associated with the Curie point. So, we conclude that under the conditions of measurements the maximum electrocaloric ΔT occurs in close vicinity of the Curie point. For the chosen experimental conditions the largest electrocaloric change in temperature is 0.75 K at 363 K under ΔE of 34 kV/cm, which agrees with previous reports on bulk ceramics [28,29]. The common wisdom rooted in Eq. (1) is that ΔT can be increased through application of high fields, which, in turn, could be achieved in high-quality thin films [1]. For this study an epitaxial BCZT thin-film heterostructure using LSMO top and bottom electrodes was fabricated on a single-crystal STO (100) substrate using a commercial pulsed-laser-deposition system [30]. Details on the film growth and characterization can be found in the Supplemental Material (see Figs. S3 and S4 [19]). The high-quality epitaxial BCZT thin film grown using PLD leads to high values of the dielectric constant (see Fig. S5 in the Supplemental Material [19]) which allowed for the application of ultrahigh fields up to 1000 kV/cm, which is a 30 times increase with respect to the bulk. The associated hysteresis loops are given in Fig. 1(d) and reveal a striking feature: the films remain in the ferroelectric phase in the entire temperature range that is much above the Curie point of 363 K. As before, the data were used within the indirect approach of Eq. (1) to estimate the electrocaloric ΔT [see Fig. 1(f)]. Surprisingly, the data reveal that despite a nearly 30 times increase in the applied electric field, the maximum ΔT has only increased 2 times. This is a very discouraging finding, as thin films are prime candidates for practical application, exactly for the reason of allowing higher field applications. Does our finding suggest that the thin-film route may not bring the desired breakthrough for solid-state cooling?

To gain an insight into such an unexpected finding, we turn to first-principles-based simulations and focus on the role that the electric field plays in the effect. The advantage of simulations is that they can assess the range of fields beyond those accessible in experiment. Figure 2 gives simulated hysteresis loops in bulk $Ba(Ti_{0.9}, Zr_{0.1})O_3$ for a different range of applied electric field, $[-E_0 : E_0]$. The data predict that the change of E_0 has a dramatic effect on the hysteresis loops. Most importantly, for the largest field range the simulated supercell exhibits ferroelectric behavior in the entire temperature range investigated, that is, beyond the computational Curie point of 410 K for the material [22]. This reproduces the unusual experimental finding reported in Fig. 1(d) and suggests that the application of ultrahigh fields could stabilize the ferroelectric phase beyond the Curie point, the effect that we term "superpoling" of the ferroelectric. We hypothesize that superpoling of a ferroelectric is similar to supercooling/superheating of a liquid. Such regimes are associated with a transient existence (sometimes brief, sometimes long) of a metastable phase at temperatures at which the chemical potential of the stable phase is lower [31]. In analogy, the superpoled state of a ferroelectric is a metastable polar phase of transient existence that persists at zero field and above the material's Curie point. For first-order phase transitions in the vicinity of the Curie point, the free energy has

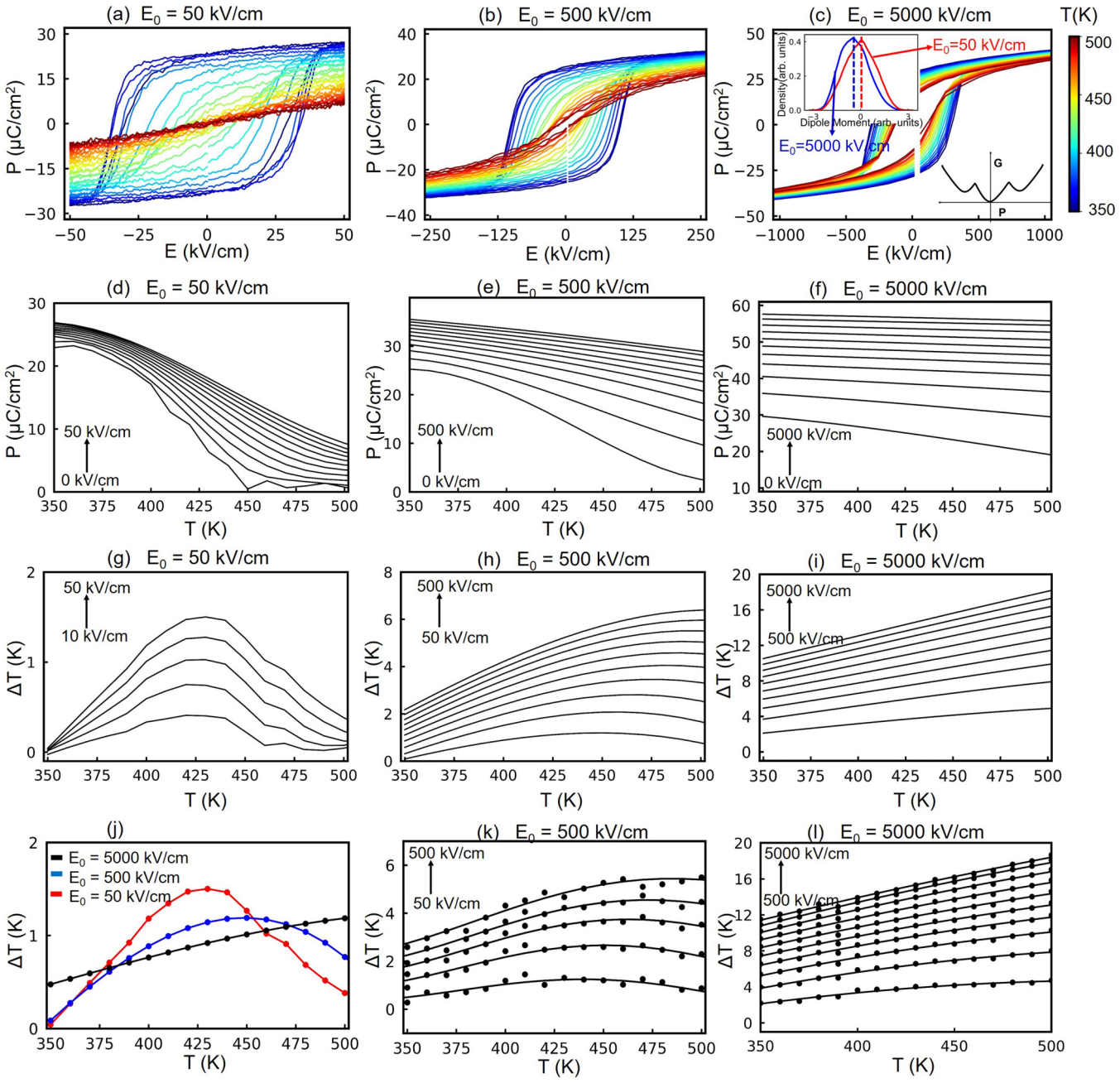

FIG. 2. Ferroelectric hysteresis loops obtained in MD simulations with different range of electric fields: [–50:50] kV/cm (a), [–500:500] kV/cm (b), and [–5000:5000] kV/cm (c). In (c) left inset gives zero-field dipole distribution function at 520 K for two different values of the poling field. Right inset is schematic free-energy landscape in the vicinity of first-order phase transition. Dependence of polarization on temperatures (d)–(f) obtained from the data of panels (a)–(c), respectively. Electrocaloric change in temperature (g)–(i) computed from dependencies of panels (d)–(f) using Eq. (1). Electrocaloric change in temperature as a function of temperature due to application of 50-kV/cm field (j). Different curves correspond to different values of the poling field as given in the legend. Electrocaloric $\Delta T(T)$ obtained from direct adiabatic simulations for different value of E_0 as given in the titles (k)–(l).

minima at $P = 0$ and $P \neq 0$ values of the order parameter [32] [see inset in Fig. 2(c)]. The metastable superpoled state is associated with $P \neq 0$ local minima. To test our hypothesis, we compute the zero-field dipole distributions at 520 K (that is, 110 K above the computational Curie point) from the simulations with $E_0 = 50$ and 5000 kV/cm. The plots are given in the inset to Fig. 2(c). For $E_0 = 50$ kV/cm the dipole distribution is symmetric and centered at $P = 0$, and the microstate corresponds to $P = 0$ global minimum of free energy. For $E_0 = 5000$ kV/cm the distribution is slightly asymmetric and centered at a finite value of polarization, the microstate corresponds to $P \neq 0$ local minimum of the free energy. These confirm that the superpoled state is the metastable state of the system. Such transient states are more likely to appear in high-purity samples or in simulations, which lack nucleation sites. Note that the slight asymmetry in $E_0 = 5000$ kV/cm data is due to the small population of dipoles in the $P = 0$ minimum of free energy.

Superpoling also affects the coercive field, as evident from Figs. 2(a)–2(c). In all cases we find the same nucleation-limited switching [33], which is mostly homogeneous nucleation of extremely small domains of opposite polarization, followed by their growth and coalescence. Distribution functions for dipole moments computed during polarization reversal reveal that the supercell passes through a $P = 0$ phase similar to the one shown in the inset of Fig. 2(c). Since superpoling temporarily "traps" the system in the $P \neq 0$ phase, larger fields are needed to get to the $P = 0$ phase, which explains the higher coercive fields in the superpoled state.

It is convenient to term the largest magnitude field that the sample experiences (either in the ac or dc regime), E_0, as the effective poling field. The strong dependence of the polarization response on this effective poling field necessitates the addition of E_0 as another variable for the polarization. In other words, the polarization is now a function of temperature, applied electric field, and the effective poling field, that is, $P(E, T, E_0)$. Interestingly, this finding suggests that for such materials Eq. (1) should be written as $\Delta T \approx -\frac{T}{\rho C_E}\int_{E_1}^{E_2}(\frac{\partial P}{\partial T})_{E,E_0}dE$, which reveals that the electrocaloric ΔT is a function of the effective poling field, $\Delta T(T, E_0, E_1, E_2)$. Integration of this expression for the $P(E, T, E_0)$ dependencies harvested in computations [see Figs. 2(a)–2(f)] gives the electrocaloric $\Delta T(T, E_0, \Delta E)$ shown in Figs. 2(g)–2(i). The data reveal a drastic change in the shape of curves as the poling field increases. The most striking feature is the dramatic shift in the position of the peak in $\Delta T(T)$. As the applied electric field increases, the peak shifts toward higher temperatures and finally moves outside of the simulated temperature range [see Fig. 2(i)]. This is exactly what happens as experimentally we switch from bulk (low $E_0 = 34.4$ kV/cm) to high-quality thin films (high $E_0 =$ 1000 kV/cm). The peak moves outside the measured range, which explains the unexpectedly low values of ΔT inside the range. An explicit demonstration of the dependence of ΔT on E_0 can be achieved through keeping ΔE constant, as it is done in Fig. 2(j), where the shift in the position of $\Delta T_{\max}$ as E_0 increases is very clear. The shift in the position of $\Delta T_{\max}$ towards higher temperature has been reported in Ref. [5], where it was found that a line of maximum electrocaloric effect passes through the zero-field ferroelectric transition, continuing along a Widom line at high temperatures with increasing fields. Our data in Figs. 2(d)–2(f) demonstrate that such a zero-field ferroelectric transition is a function of the poling field, which explains the shift in the position of $\Delta T_{\max}$ as a function of E_0 for low ΔE [Figs. 2(g)–2(i)].

After these demonstrations one may wonder if the role of the hidden variable E_0 is enhanced (or even introduced in the first place) by the application of the indirect approach of Eq. (1). To answer this question we carried out direct simulations of the electrocaloric effect using both adiabatic semiclassical Monte Carlo (MC) [26] and isothermal MD [27] approaches as detailed in Sec. II. Data from direct adiabatic simulations are presented in Figs. 2(k)–2(l) and demonstrate good agreement with predictions from the indirect approach. Data from direct isothermal simulations are given in the Supplemental Material (see Fig. S6 [19]) and are in agreement with both indirect predictions and direct adiabatic simulations. Consequently, direct simulations confirm the trends found in the indirect predictions. In particular, we find a dependence on the effective poling field in both types of direct simulations and conclude that the effects reported here are not introduced by the application of the indirect methodology. We would also like to note that we have previously demonstrated that direct and indirect approaches provide identical results if the data from the same branch of hysteresis loop are used and the irreversible regions around the coercive field are excluded [34]. All of our indirect data are within the region of the indirect approach validity.

Having achieved the understanding of the role that poling plays in the electrocaloric ΔT, we now aim to manipulate E_0 in order to enhance the electrocaloric effects in our films. Figure 2 suggests that it should be possible to shift the position of the peak in ΔT to lower temperatures by reducing the effective poling field and avoiding superpoling. We repeated our experiment on the same film but with a reduced electric field of 500 kV/cm. The data are given in Fig. 3 and demonstrate that, indeed, reducing the electric field brings the position of $\Delta T_{\max}$ within the temperature range of the measurements (and close to the Curie temperature of bulk). This results in a seven times enhancement of largest ΔT value in the given temperature range as compared to the high-field data. This finding not only demonstrates the possibility to manipulate the electrocaloric effect by the effective poling field but also reveals a counterintuitive enhancement of the electrocaloric effect through the reduction of electric field. The value of $\Delta T_{\max} = 8.5$ K is in the range of computational predictions from a direct adiabatic approach of 5.4–7.2 K for applied fields of 500–800 kV/cm which are below the superpoling regime in computations (Fig. S7 in the Supplemental Material [19]). Figure 3(d) shows the dependence of the largest ΔT on the applied field (the case of $E_0 = \Delta E$) from the hysteresis loops measured on the film (see also Fig. S8 of Supplemental Material [19]). Below 500 kV/cm, $\Delta T_{\max}$ increases with field. Above this value we find that the largest ΔT decreases as a function of field as the superpoled regime sets at 1000 kV/cm. The position of the peak in $\Delta T(T)$ reported in the same figure shifts towards higher temperatures for all fields.

We note that our experimental thin films are under small compressive strain of –0.15% (see Supplemental Material [19]), which may further contribute to the stabilization of the ferroelectric phase above the bulk T_C [35–37] and associated decrease in ΔT. For example, we found out in computations under compressive strain of –0.22% strain with respect to cubic lattice constant that the Curie temperature increases by 30 K, causing the peak in $\Delta T(T)$ to shift towards higher temperatures. Comparison between $\Delta T_{\max}$ for the same E_0 and ΔE for the unstrained and strained supercells reveals a slight enhancement due to compressive strain (see Fig. S9 of the Supplemental Material [19]). Nevertheless, strain by itself cannot account for our main findings. Indeed, the measurements carried out on the same film under different fields [see Figs. 1(d) and 3(a)] fix the strain while demonstrating significant dependence of both hysteresis loops and electrocaloric ΔT on the poling field.

One may wonder if the effects reported here are common for ferroelectrics or just specific for the material we considered. To gain some insight we repeated simulations for

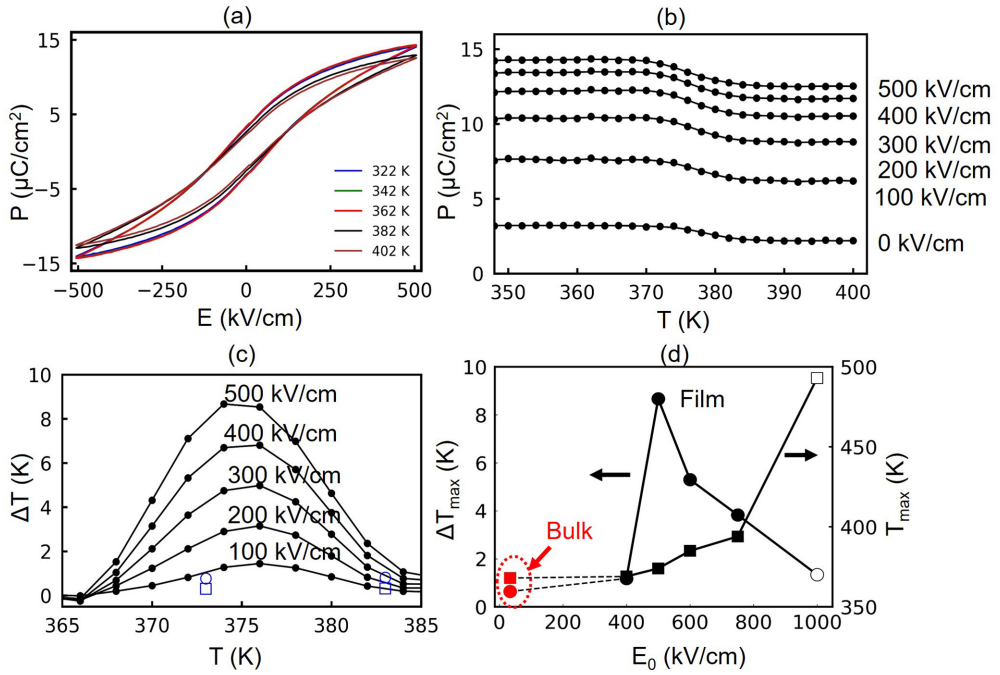

FIG. 3. Hysteresis loops (a) and associated temperature dependence of polarization (b) in 100-nm BCZT thin film for poling field of 500 kV/cm. Electrocaloric ΔT computed from experimental data using the approach of Eq. (1) (c). For comparison we include data for $E_0 = 1000$ kV/cm and $\Delta E = 100$ kV/cm (blue squares) and 500 kV/cm (blue circles). The peak electrocaloric temperature ΔT_{max} and its position T_{max} as a function of the poling field for the case $E_0 = \Delta E$ for both bulk ceramics and thin film (d). Open symbols correspond to the largest values in the given temperature range when the peak is outside the range.

$BaTiO_3$, which is a prototypical ferroelectric. Surprisingly, we found the aforementioned dependencies on E_0 to hold even in this material (see Fig. S10 in the Supplemental Material [19]), which provides evidence that they are likely to be common to ferroelectrics. Of course, some ferroelectrics could have only weak dependence on E_0, while others could have a strong one, like the one we considered in this study.

IV. CONCLUSIONS

In summary, we have reported that the electrocaloric effect in ferroics exhibits a strong and counterintuitive dependence on the effective poling field, which can be viewed as a "hidden" variable of the caloric effect. This hidden variable becomes extremely powerful at the nanoscale, where fields could reach thousands of kV/cm and could lead to "superpoling" of thin films. Once superpoled, the films exhibit ferroelectric behavior much above the material's Curie point, which causes deterioration of the caloric response. On the positive side, this uncovered dependence on the effective poling field is an additional "knob" for the electrocaloric effect, which could be used for its enhancement. For example, we demonstrated that a two times reduction of electric field results in seven times enhancement of the electrocaloric effect. As ferroics in general exhibit similar properties, we expect that our findings would apply to this class in general and, therefore, are likely to bring new light into the entire family of caloric effects: magnetocaloric, barocaloric, multicaloric, and others, in addition to the electrocaloric effects considered here.

ACKNOWLEDGMENTS

The computational work is supported by the U.S. Department of Energy, Office of Basic Energy Sciences, Division of Materials Sciences and Engineering under Grant No. DE-SC0005245. D.M. acknowledges funding from the Technical Research Center, Department of Science and Technology, Government of India (Grant No. AI/1/62/IACS/2015), and a Science and Engineering Research Board (SERB) Starting Research Grant, Government of India (Grant No. SRG/2019/000387). A.D. acknowledges funding from a SERB-Ramanujan Fellowship (Award No. SB/S2/RJN-057/2017) and a SERB-Core Research Grant (Grant No. CRG/2020/002395). S.K.-N. acknowledges funding from a European Research Council Starting Grant (Grant No. ERC-2014-STG-639526, NANOGEN). S.C. acknowledges a research fellowship from DST-INSPIRE, Government of India. A.B. acknowledges a research fellowship from CSIR-UGC, Government of India. S. B. thanks CSIR-India for a research fellowship.

[1] A. S. Mischenko, Q. Zhang, J. F. Scott, R. W. Whatmore, and N. D. Mathur, Science **311**, 1270 (2006).

[2] A. S. Mischenko, Q. Zhang, R. W. Whatmore, J. F. Scott, and N. D. Mathur, Appl. Phys. Lett. **89**, 242912 (2006).

[3] Y. Bai, G. Zheng, and S. Shi, Appl. Phys. Lett. **96**, 192902 (2010).

[4] B. Peng, H. Fan, and Q. Zhang, Adv. Funct. Mater. **23**, 2987 (2013).

[5] M. C. Rose and R. E. Cohen, Phys. Rev. Lett. **109**, 187604 (2012).

[6] H.-J. Ye, X.-S. Qian, D.-Y. Jeong, S. Zhang, Y. Zhou, W.-Z. Shao, L. Zhen, and Q. M. Zhang, Appl. Phys. Lett. **105**, 152908 (2014).

[7] A. Kumar, A. Thakre, D.-Y. Jeong, and J. Ryu, J. Mater. Chem. C **7**, 6836 (2019).

[8] J. Li, Y. Chang, S. Yang, Y. Tian, Q. Hu, Y. Zhuang, Z. Xu, and F. Li, ACS Appl. Mater. Interfaces **11**, 23346 (2019).

[9] S. E. Shirsath, C. Cazorla, T. Lu, L. Zhang, Y. Y. Tay, X. Lou, Y. Liu, S. Li, and D. Wang, Nano Lett. **20**, 1262 (2020).

[10] M. Li, S. Han, Y. Liu, J. Luo, M. Hong, and Z. Sun, J. Am. Chem. Soc. **142**, 20744 (2020).

[11] X. Moya and N. D. Mathur, Science **370**, 797 (2020).

[12] A. Torelló, P. Lheritier, T. Usui, Y. Nouchokgwe, M. Gérard, O. Bouton, S. Hirose, and E. Defay, Science **370**, 125 (2020).

[13] I. Takeuchi and K. Sandeman, Phys. Today **68**, 48 (2015).

[14] A. Barman, S. Kar-Narayan, and D. Mukherjee, Adv. Mater. Interfaces **6**, 1900291 (2019).

[15] Y. Bai, G.-P. Zheng, K. Ding, L. Qiao, S.-Q. Shi, and D. Guo, J. Appl. Phys. **110**, 094103 (2011).

[16] R. Su, D. Zhang, Y. Liu, J. Lu, Z. Wang, L. Li, J. Bian, M. Wu, X. Lou, and Y. Yang, Phys. Chem. Chem. Phys. **18**, 29033 (2016).

[17] F. Guo, X. Wu, Q. Lu, and S. Zhao, Ceram. Int. **44**, 2803 (2018).

[18] G. Zhang, X. Zhang, T. Yang, Q. Li, L.-Q. Chen, S. Jiang, and Q. Wang, ACS Nano **9**, 7164 (2015).

[19] See Supplemental Material at http://link.aps.org/supplemental/10.1103/PhysRevMaterials.6.124403 for bulk BCZT ceramic preparation, x-ray diffraction (XRD), energy-dispersive spectroscopy (EDS), x-ray photoelectron spectroscopy (XPS) and Raman spectroscopy, temperature-dependent dielectric and ferroelectric measurements, and thin-film fabrication and characterization. Computational details, data from direct isothermal and adiabatic simulations, effect of strain on electrocaloric effect.

[20] A. Barman, S. Chatterjee, J. K. Dey, A. Datta, and D. Mukherjee, Phys. Rev. B **102**, 054433 (2020).

[21] A. Barman, S. Chatterjee, C. Ou, Y. Yau Tse, N. Banerjee, S. Kar-Narayan, A. Datta, and D. Mukherjee, APL Mater. **9**, 021115 (2021).

[22] C. Mentzer, S. Lisenkov, Z. G. Fthenakis, and I. Ponomareva, Phys. Rev. B **99**, 064111 (2019).

[23] D. C. Rapaport and D. C. R. Rapaport, *The Art of Molecular Dynamics Simulation* (Cambridge University Press, Cambridge, England, 2004).

[24] P. Virtanen, R. Gommers, T. E. Oliphant, M. Haberland, T. Reddy, D. Cournapeau, E. Burovski, P. Peterson, W. Weckesser *et al.*, Nat. Methods **17**, 261 (2020).

[25] D. Liu, Q. Li, and Q. Yan, CrystEngComm **20**, 1597 (2018).

[26] P. Jouzdani, S. Cuozzo, S. Lisenkov, and I. Ponomareva, Phys. Rev. B **96**, 214107 (2017).

[27] S. Lisenkov and I. Ponomareva, Phys. Rev. B **97**, 184104 (2018).

[28] J. Wang, T. Yang, S. Chen, G. Li, Q. Zhang, and X. Yao, J. Alloys Compd. **550**, 561 (2013).

[29] Z. Hanani, S. Merselmiz, D. Mezzane, M. Amjoud, A. Bradeško, B. Rožič, M. Lahcini, M. El Marssi, A. V. Ragulya, I. A. Luk'yanchuk, Z. Kutnjak, and M. Gouné, RSC Adv. **10**, 30746 (2020).

[30] S. Chatterjee, A. Barman, S. Barman, T. Chabri, S. Kar-Narayan, A. Datta, and D. Mukherjee, Phys. Rev. Mater. **5**, 064415 (2021).

[31] C. Kittel, *Introduction to Solid State Physics*, 6th ed. (John Wiley & Sons, Inc., New York, 1986).

[32] K. M. Rabe, K. M. Rabe, C. H. Ahn, and J.-M. Triscone, *Physics of Ferroelectrics: A Modern Perspective*, 1st ed. (Springer Publishing Company, Incorporated, New York, 2007).

[33] A. K. Tagantsev, I. Stolichnov, N. Setter, J. S. Cross, and M. Tsukada, Phys. Rev. B **66**, 214109 (2002).

[34] M. Kingsland, S. Lisenkov, and I. Ponomareva, Adv. Theor. Simul. **1**, 1800096 (2018).

[35] F. He and B. O. Wells, Appl. Phys. Lett. **88**, 152908 (2006).

[36] K. J. Choi, M. Biegalski, Y. L. Li, A. Sharan, J. Schubert, R. Uecker, P. Reiche, Y. B. Chen, X. Q. Pan, V. Gopalan, L.-Q. Chen, D. G. Schlom, and C. B. Eom, Science **306**, 1005 (2004).

[37] D. G. Schlom, L.-Q. Chen, C.-B. Eom, K. M. Rabe, S. K. Streiffer, and J.-M. Triscone, Annu. Rev. Mater. Res. **37**, 589 (2007).